Check for updates

IET
The Institution of Engineering and Technology WILEY

ORIGINAL RESEARCH PAPER

An isolated-boost-converter-based unidirectional three-phase off-board fast charger for electric vehicles

Ahmed Elserougi[1] | Ibrahim Abdelsalam[2] | Ahmed Massoud[3]

[1]Department of Electrical Engineering, Alexandria University, Alexandria, Egypt

[2]Electrical Engineering Department, Arab Academy for Science Technology & Maritime Transport, Cairo, Egypt

[3]Department of Electrical Engineering, Qatar University, Doha, Qatar

Correspondence

Ahmed Elserougi, Department of Electrical Engineering, Alexandria University, Alexandria, Egypt.
Email: ahmed.elserougi@alexu.edu.eg

Abstract

In this work, a novel three-phase unidirectional off-board Electric Vehicles (EVs) fast charger is proposed. Each phase of the proposed converter consists of a two-stage converter. The first stage is an AC–DC front-end converter with power factor correction (PFC) control. The front-end AC–DC converter is based on an isolated boost converter, which has a boosting capability and provides galvanic isolation. In this stage, parallel-in parallel-out isolated boost converter modules are employed in each phase. This enables sharing the current among modules to avoid implementing one module with a high current rating to meet the fast-charging requirements. The multimodule option provides fault-ride through capability for the proposed charger. The DC outputs of involved phases, that is, three isolated DC voltages, are fed to three cascaded DC–DC unidirectional buck converters. The charging terminals are used to charge the EV battery through a filter inductor with a charging current controller's aid. A detailed illustration of the suggested closed-loop controllers is presented to ensure a successful operation for the proposed architecture. A simulation case study for a 25-kW charger is presented. Finally, a 1-kW prototype is implemented for experimental validation.

KEYWORDS

battery chargers, electric vehicle charging

1 | INTRODUCTION

The transition from oil-based vehicles to Electric Vehicles (EVs) increased in the past few decades due to the EVs' salient advantages such as fuel cost elimination, and vehicle emissions reduction helping the environment [1].

The U.S. Department of Energy has classified EVs' charging into three levels: levels 1, 2, and 3. Level 1 is mainly a slow/standard charging, which uses single-phase AC input, and the charger power rating is less than 5 kW. Level 2 is a fast-charging that uses three-phase AC input, and the charger power rating is between 5 and 50 kW. Finally, level 3 is a super-fast charging with a power rating above 50 kW [2, 3].

The fast-charging level is the main focus of this paper. The fast chargers are suitable for batteries capable of accepting high charging rates (up to 10 C) with high charging cycles [3].

Unidirectional and bidirectional chargers are the main types of EV chargers based on the charger circuit's available/allowable power flow directions. The unidirectional charger has a single power flow direction from the electric grid to the EVs battery, that is, it cannot inject energy to the power grid. On the other hand, the bidirectional charges provide power flows from grid to vehicle (G2V), that is, charging mode, and from vehicle to grid (V2G), that is, discharging mode [4–7]. The chargers can also be classified into on-board or off-board chargers based on the charger's location inside or outside the vehicle, respectively. It has to be noted that a fast unidirectional off-board charger is the main focus of the presented work.

Different EVs chargers' topologies were proposed in the literature [8–18], where generally the charger consists of a front-end AC–DC converter followed by a DC–DC converter [19, 20], where a high-frequency transformer can be employed when needed to provide the required isolation

[13, 19]. The AC–DC converter should draw sinusoidal currents from the power grid to ensure operating with an acceptable power quality level. Generally, boost-converter-based power factor correction (PFC) is commonly used with the EV chargers [8, 9], where an uncontrolled rectifier is used, followed by a boost converter to achieve the PFC task. Alternatively, bridgeless boost PFC can be employed effectively [10]. Single boost-converter or interleaved boost converters can be employed in the PFC stage. The interleaved boost converter supports current sharing among the interleaved converters and reduces boost converter input inductance [11, 12]. Multilevel converters can be employed for high-power chargers, as presented in Ref. [13]. The multilevel converter-based chargers' main advantage is employing semiconductor devices with a low-voltage rating for a high-power converter but at the cost of converter control complexity. Moreover, three-phase multilevel converters provide operation with sinusoidal AC currents with reduced total harmonic distortion and reduced EMI noise [14]. In Ref. [15], SEPIC DC–DC converter-based three-phase fast charger has been presented with discontinuous conduction mode operation. In this topology, multimodule option can be applied, that is, parallel modules per-phase can be used for current sharing purpose. The topology, presented in Ref. [15], has a low number of controlled semiconductors but is rated at a relatively higher voltage than the other topologies. It also has a large number of passive elements (inductors and capacitors) rated at a higher voltage. Finally, an LCL filter is needed at the AC side. Also, in Ref. [16], a unidirectional three-phase SEPIC-based PFC rectifier has been presented. It has a large number of components with reduced voltage stresses on the involved components, but it has no galvanic isolation, and it requires an input AC filter. In Ref. [17], an interleaved isolated PFC converter module for three-phase EV chargers has been presented for wide output voltage ranges. The topology has two half-bridge voltage-fed isolated PFC converters with a parallel-input-series-output configuration where interleaved discontinuous conduction mode is used. A higher number of semiconductor devices is needed in this topology. In Ref. [18], a bidirectional PFC converter with a soft-switching operation has been presented. The bidirectional option is essential to provide the ability to operate in Vehicle-to-Grid (V2G) and Grid-to-Vehicle (G2V) modes. In unidirectional chargers, only G2V operational mode is available. A detailed review of the different types of unidirectional and bidirectional charges can be found in Ref. [21].

In this work, a novel three-phase unidirectional off-board fast charger for EVs is proposed. The converter is based on parallel-in parallel-out isolated boost converters per-phase as a front-end AC–DC converter stage with PFC control followed by cascaded DC–DC buck converters for the DC–DC conversion stage. The proposed charger provides current sharing among the involved parallel-in parallel-out isolated boost converter modules to meet the fast-charging approach's high current requirement while employing isolated boost converter modules with a relatively low current rating. Besides, the modular multilevel converter (MMC) cells selection concept is employed in the DC–DC conversion stage with the cascaded DC–DC buck converters to generate the proper output voltage needed for the battery's charging process. The closed-loop controllers of the suggested approach are presented to ensure the successful operation of the suggested approach. The operation provides balanced three-phase currents at the AC grid side, balanced capacitors voltages at the isolated boost converter output stages and injecting the desired current level into the EV battery.

The proposed approach has a low number of passive elements (inductors and capacitors), which positively affects the charger cost and size. It also has a high number of semiconductor devices but with a lower voltage rating. In addition, in case of one- or two-phase loss, the proposed architecture can continue operating successfully with the other healthy phases. A simulation case study for a 25-kW charger is presented while a scaled-down prototype (1 kW) is implemented for validation.

2 | THE PROPOSED FAST EVs CHARGER

The proposed three-phase unidirectional EV charger is shown in Figure 1, where each phase of the involved three phases consists of two cascaded stages. The first stage is a parallel-in parallel-out isolated boost converter, where the current is shared among isolated boost converter modules. The per-module transformer provides the isolation between the supply and the load side. The second stage is a DC–DC buck converter used to insert/bypass the boost converter output voltage in/from the battery charging loop at the output terminals. For the three-phase arrangement shown in Figure 1, three DC–DC cascaded buck converters with isolated DC sources are employed for the battery charging process. It looks like the MMC arm with three unidirectional half-bridge submodules (UHBSMs) and has the same operating concept of submodules insertion or bypassing decision. This structure is suggested to integrate three isolated DC voltages to feed the battery load through these buck converters with proper control.

To ensure drawing AC current with good quality from the AC grid at unity power factor, the isolated boost converter inductors' currents are controlled to ensure having a rectified AC current passing through them at unity supply power factor (Power Factor Correction (PFC) feature). Inductor currents' proper magnitudes are extracted from the closed-loop control on the boost converters' output voltages (capacitors voltages) to keep them constant with the loading during the charging process.

The charging loop at the output terminals is controlled to ensure that the charging current (I_{Bat}) tracks its reference value, that is, constant current charging (CC) is employed. This can be done by measuring the battery current and compare it with its reference value. The current error is then fed to a conventional PI controller to extract the output voltage's reference value (V_o) shown in Figure 1.

FIGURE 1 The proposed three-phase fast charger for electric vehicles
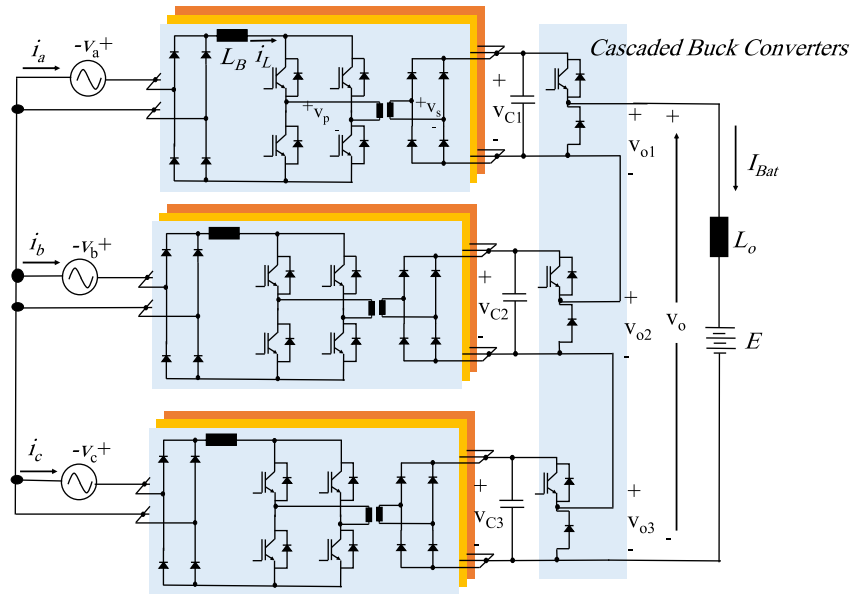
Based on the extracted (V_o) reference, proper capacitors of the involved DC–DC buck converters are inserted in the battery charging loop using a proper multilevel PWM technique to generate the desired overall output voltage at the charging terminals, namely V_o. Meanwhile, the voltages of the capacitors (V_{C1}–V_{C3}) should be kept under the same loading condition to ensure drawing balanced AC current from the three-phase source. Like MMC control approach, this can be done by employing a proper voltage balancing technique for the involved cascaded buck converters.

It has to be noted that in case of one- or two-phase loss, the proposed architecture can continue operating successfully with the other healthy phases but with a higher V_{Cref} (higher boosting ratio) and modified charging current control loop. In this case, the buck converter of the lost phase is bypassed by turning off its upper IGBT and continue the operation with the other submodules.

3 | CONTROL SYSTEM

The control system of the proposed three-phase EVs charger is divided into two main controllers, namely, the PFC controller and charging current controller, which can be illustrated as follows.

3.1 | PFC control

The PFC control is applied for each isolated boost converter module of the involved modules, where the per-module PFC controller is shown in Figure 2. The PFC controller is responsible for drawing sinusoidal current from the AC grid and maintaining the capacitor voltage at the output stage constant at a particular voltage level. This can be done by applying PI-based closed-loop voltage control

on the module output capacitor to determine the rectified AC current's suitable peak to be passed through the boost converter module's inductor. It has to be noted that this rectified current should be synchronized with the module AC input voltage by applying the technique shown in Figure 2 to ensure drawing AC current from the AC grid at unity power factor. By applying closed-loop control on the inductor current, the gating pulses of the boost converter switches (S_1 to S_4) can be extracted as shown in Figure 2, where a closed-loop hysteresis current controller is employed in the shown PFC controller scheme. It has to be noted that the switches (S_1, S_2, S_3, S_4) are turned on during the inductor charging. Meanwhile, the transformer primary winding is shorted.

During discharging period, the operation is swapped between enabling (S_1, S_2) and enabling (S_3, S_4), that is, to have positive and negative primary transformer voltage, respectively, with zero average voltage, which enables better utilization of the involved transformer. This can be done by the logic circuit shown in the right-hand side of Figure 2, where a square wave signal with periodic time $1/f_{trans}$ is used to enable the aforementioned swapping technique. The frequency is selected relatively high (i.e. few kHz) to ensure operating with a reduced size transformer, that is, operating with the advantages of a high-frequency transformer.

3.2 | Charging current control

The charging (load) current should be appropriately controlled to ensure injecting the desired charging current into the battery during the CC charging mode. The proposed closed-loop current controller is shown in Figure 3, where a PI-based closed-loop control on the charging (load) current is applied to generate the suitable voltage to be applied at the charging terminals, namely, V_o.
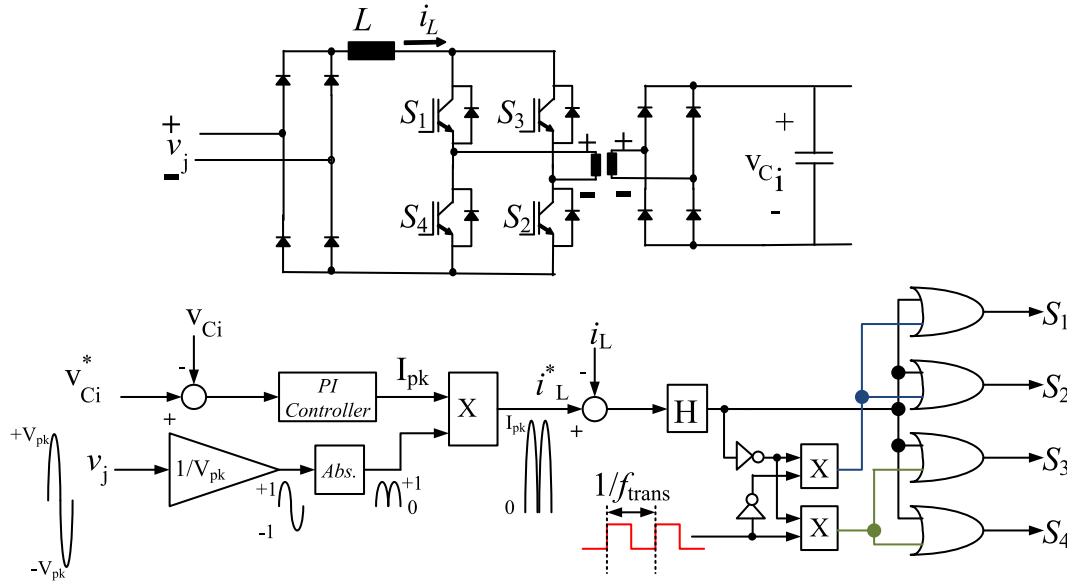
FIGURE 2 Per-module power factor correction controller to ensure drawing sinusoidal current from the AC grid while keeping constant capacitor voltage
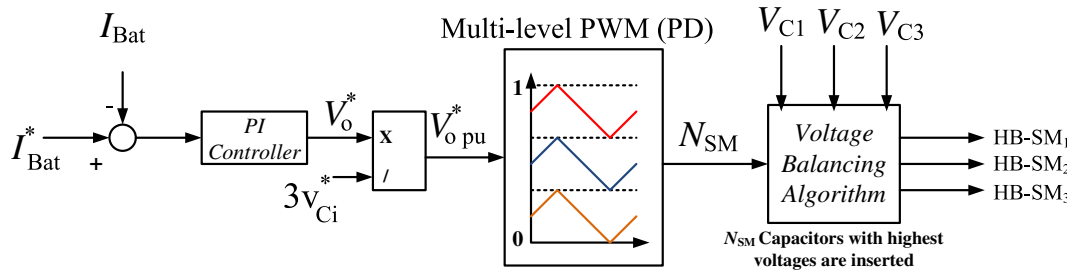

FIGURE 3 Charging current control during normal operating conditions to ensure injecting the desired battery current and drawing balanced three-phase AC currents from the AC grid

Based on the extracted V_o voltage, a multilevel PWM technique such as the phase disposition modulation technique activates some of the three involved UHBSMs and bypasses others based on the V_o voltage level. To decide which UHBSM to be activated and bypassed with the operation, the voltage-balancing algorithm should be employed to ensure equal loading on the involved capacitors, hence operating with three-phase balanced AC currents. In the voltage balancing algorithm, first, the capacitors' voltages are sorted. Then, based on the PWM technique, the number of activated SMs (N_{sm}) is known, so N_{sm} UHBSMs with higher capacitors voltages are activated, that is, their capacitors are inserted in the charging loop to discharge their energy into the battery. It has to be noted that the PFC control replenishes the capacitors' voltages again with the operation. That is why keeping equal loading of the three involved UHBSMs at the charging loop results in drawing balanced three-phase AC current from the grid. If the voltage balancing algorithm is not applied, and the involved capacitors are not equally loaded, AC currents with unequal magnitudes will be drawn from the AC grid (i.e. unbalanced operation), which is not recommended. Applying a voltage balancing algorithm is essential in the proposed approach to ensure drawing balanced three-phase currents from the AC grid.

3.3 | Block diagram of the control

The block diagram of the proposed approach is shown in Figure 4, where $G_V(s)$ represents the transfer function of the capacitor voltage controller, $G_i(s)$ represents the transfer function of the inductor current controller, $H_i(s)$ represents duty-to-inductor current transfer function of the boost converter, $H_V(s)$ represents inductor current-to-output voltage transfer function of the boost converter, and $G_{ib}(s)$ represents the transfer function of the battery current controller. Based on [22], the transfer functions $H_i(s)$ and $H_V(s)$ are given by Equations (1) and (2) where V_C is the capacitor voltage, V_{in} is the boost converter input voltage, L_B is the equivalent boost converter inductor, and R_{eq} is the equivalent resistance seen by the output capacitance C.
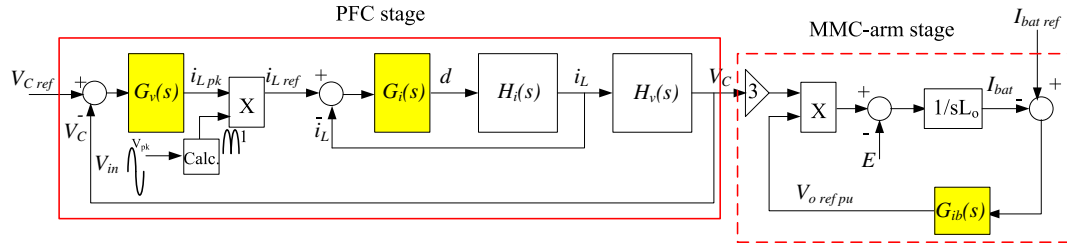
$$H_i(s) = \frac{V_C}{sL_B} \tag{1}$$

FIGURE 4 The block diagram of the control system

$$H_V(s) = \frac{R_{eq}}{R_{eq}Cs + 1} \frac{V_{in}}{V_C} \quad (2)$$

On the other hand, the transfer function of the involved controllers depends on the controller type. For a proportional–integral controller (PI-controller), the transfer function of the controller is given by

$$G(s) = K_p + \frac{K_i}{s} \quad (3)$$

where K_p and K_i are the controller gains. The block diagram shown in Figure 4 can be used to design the controller gains.

4 | SIMULATION

4.1 | Simulation results

A simulation model has been built for a 25-kW three-phase EVs charger to check and validate the proposed architecture behaviour. The simulated 25-kW charger parameters are given in Table 1, where three-phase input (220 V-phase, 50 Hz) is used to charge a 480-V battery through the proposed architecture with the suggested control system. In the simulated case study, each phase consists of two parallel-in parallel-out isolated boost converters to share the current between them, that is, each module processes 50% of the phase power. In the simulated case study, the reference capacitor voltage is 200 V while the charging current reference is 50 A, where the constant current charging method is considered in the presented work. It has to be noted that an ideal AC voltage source is assumed to simulate the AC grid while an ideal DC voltage source is used to simulate the battery.

The corresponding simulation results are shown in Figure 5. Figure 5a shows the phase voltages of the AC grid, whereas Figure 5b shows the three-phase AC current drawn from the AC grid. The drawn currents are balanced and sinusoidal with a percentage total harmonic distortion (%THD) of 4.92%. The per-phase voltage and current of the AC grid are shown in Figure 5c, where the voltage and current are in-phase (approximately 0.9983 power factor is achieved). The peak current at the AC grid is approximately 54 A under the full-load condition. The corresponding per-phase per-module inductor current is shown in Figure 5d, a rectified AC current with a peak of 27 A and synchronized with its input phase

TABLE 1 Simulation parameters

Parameter	Value
Charger rated power	25 kW
Input three-phase voltage	220-V phase, 50 Hz
Isolated boost converter	$L = 10$ mH, transformer 1:0.5, output $C = 3$ mF, hysteresis current control
f_{trans}	1 kHz
Number of boost converters/phase	2
Output inductance	5 mH
Capacitances reference voltage	200 V
PWM carrier frequency	5 kHz
Battery voltage, E	480 V

voltage. It has to be noted that the 27-A peak represents the grid current peak (54 A) divided by 2, where two parallel modules are employed per phase in the presented case study to share the current equally between them.

Figure 5e shows the per-phase per-module secondary voltage of the involved 1:0.5 transformer. The voltage is AC voltage with zero average, and the swapping between the positive and negative secondary voltage has a periodic time of $1/f_{trans}$, where f_{trans} is one of the defined parameters (1 kHz). The secondary voltage is applied to the diode bridge rectifier to replenish the voltage of output capacitance at the same phase. The corresponding capacitors voltages are shown in Figure 5f, where balanced capacitors voltages are provided with the suggested operational mode. The average value of the capacitors' voltages is equal to the capacitor reference value, ensuring the employed closed-loop voltage controller's effectiveness. Figure 5g shows the voltage at the charging terminals V_o, which is needed to ensure injecting the desired current (50 A) into the battery to be charged. Closed-loop current control at the charging loop is employed to generate the suitable voltage to be applied across the charging terminals (V_o^*). By using the PD modulation technique, a number of UHBSMs to be activated are extracted. The variation of the number of UHBSMs to be activated with the presented case study's operation is shown in Figure 5h. The voltage-balancing algorithm is responsible for selecting proper UHBSMs to activate them and bypass the others to ensure equal loading of capacitors during the operation, to ensure balanced
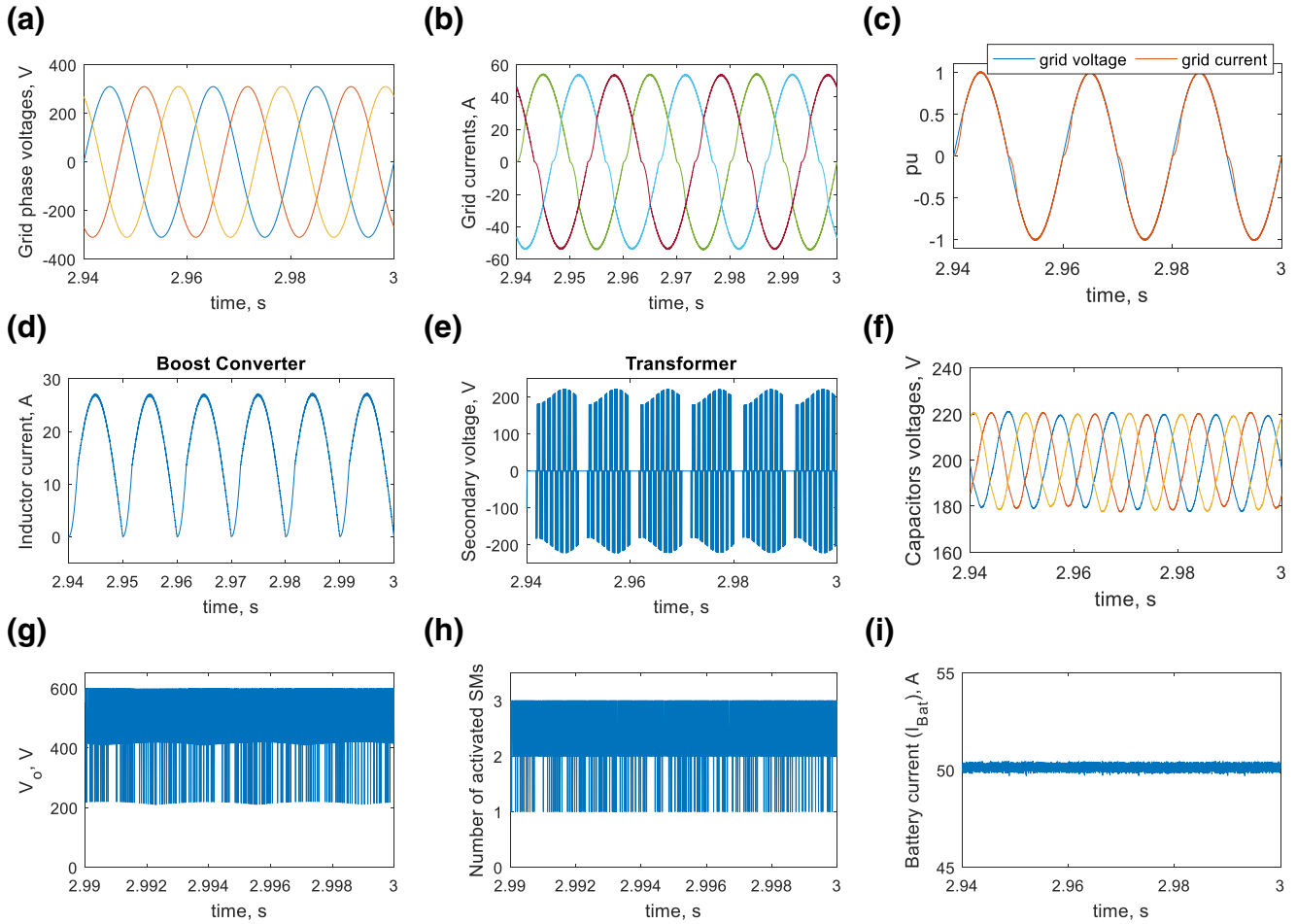
FIGURE 5 The simulation results of the proposed electric vehicles fast charger. (a) Grid phase voltages, (b) grid currents, (c) grid voltage and current of phase A, (d) boost converter inductor current of phase A modules, (e) transformer secondary voltage of phase A modules, (f) voltages of boost converters output capacitors, (g) the overall output voltage at the charging terminals, namely V_o, (h) number of activated buck converter submodules and (i) the charging current injected to the battery

AC current drawn from the AC grid as a reflection of equal loading of the involved phases, that is, ensure operating with balanced AC currents at the AC grid side.

Finally, Figure 5i shows the injected charging current, which tracks the desired charging current (50 A), which shows the effectiveness of the employed closed-loop current controller at the load side. The injected current has an average of 50 A with approximately 1% current ripple with a 5-kHz frequency.

4.2 | Converter power loss assessment

The power flow diagram of the proposed charger is shown in Figure 6a, assuming the specifications of the simulated case study given in Table 1. In this section, the efficiency of the system is assessed. The different types of losses are calculated. This includes the four diodes of the full-bridge rectifier, the copper losses of the boost converter inductor (L_B), the four semiconductor devices, the high-frequency transformer, the four diodes at the secondary side of the high-frequency transformer, losses of the cascaded buck-converters, and finally, the copper losses of the output inductor (L_o).

The main two types of losses considered are as follows.

Switching losses are due to the effort conducted for transitions between ON and OFF states of the semiconductor devices. Switching losses are directly proportional to the switching frequency, and are given by

$$P_{sw} = f_{sw}(E_{ON} + E_{OFF}) \qquad (4)$$

with E_{ON} and E_{OFF} are energy losses of the semiconductor device obtained from the relevant data sheet.

Conduction losses of semiconductor devices are generally expressed as

$$P_{con} = I_{rms}^2 R_{ON} + \alpha I_{ave} V_{ON} \qquad (5)$$

where I_{rms} and I_{ave} are the rms and average of the semiconductor device current, respectively, V_{ON} is the ON-state voltage drop, R_{ON} is the semiconductor ON-state resistance, and $\alpha = 0$ in case of MOSFET; otherwise, $\alpha = 1$.

The ohmic/copper losses of the involved inductor can be estimated simply in terms of the rms of the inductor current and the inductor effective series resistance (ESR) as follows:
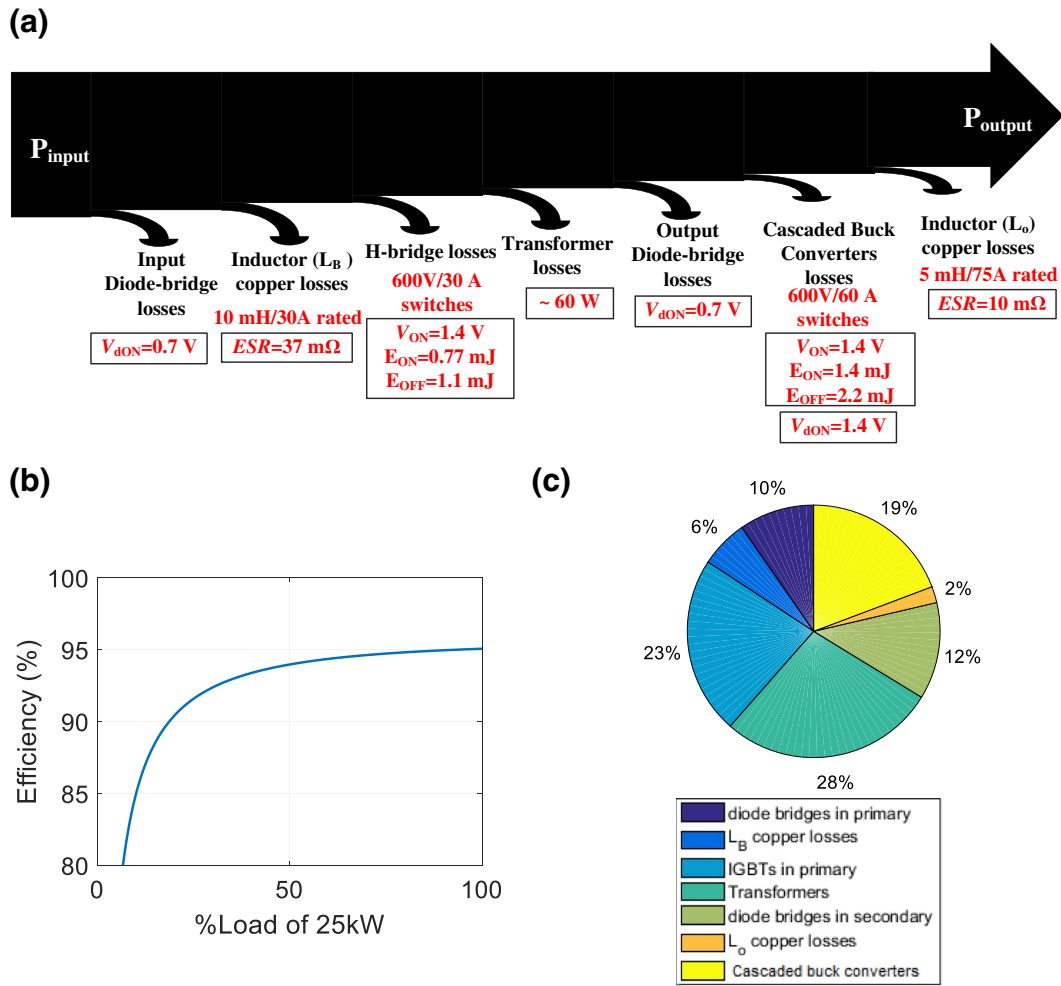
(a)

(b)

(c)

FIGURE 6 Efficiency assessment of the proposed charger. (a) The power flow diagram of the proposed charger for the simulated case study, (b) corresponding efficiency versus loading and (c) the power loss breakdown under the full-load condition
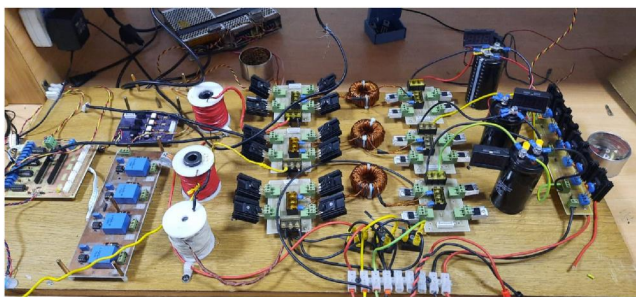

FIGURE 7 The experimental rig

$$P_{cu} = I_{L\ rms}^2 ESR \qquad (6)$$

where $I_{L\ rms}$ is the root-mean-square (rms) value of the inductor current.

The efficiency is studied considering the data shown in Figure 6a, where 30 A–600 V IGBT are employed for the primary-side IGBTs and 60 A–600 V IGBT are employed for the secondary-side IGBTs, and 30 A–600 V diodes are used in both sides. The efficiency curve is plotted versus loading in Figure 6b,

TABLE 2 Experimental parameters

Parameter	Value
Charger rated power	1 kW
Input three-phase voltage	86 V line-to-line, 50 Hz
Isolated boost converter	L = 3 mH, transformer 1:1, output C = 2.2 mF, 40 kHz
f_{trans}	10 kHz
Number of boost converter modules per phase	1
Output inductance	11 mH
Capacitances reference voltage	100 V
Load	Resistive load of 83 Ω

where an efficiency of 95% is extracted under the full-load condition. The power-loss breakdown under the full-load condition is shown in Figure 6c.
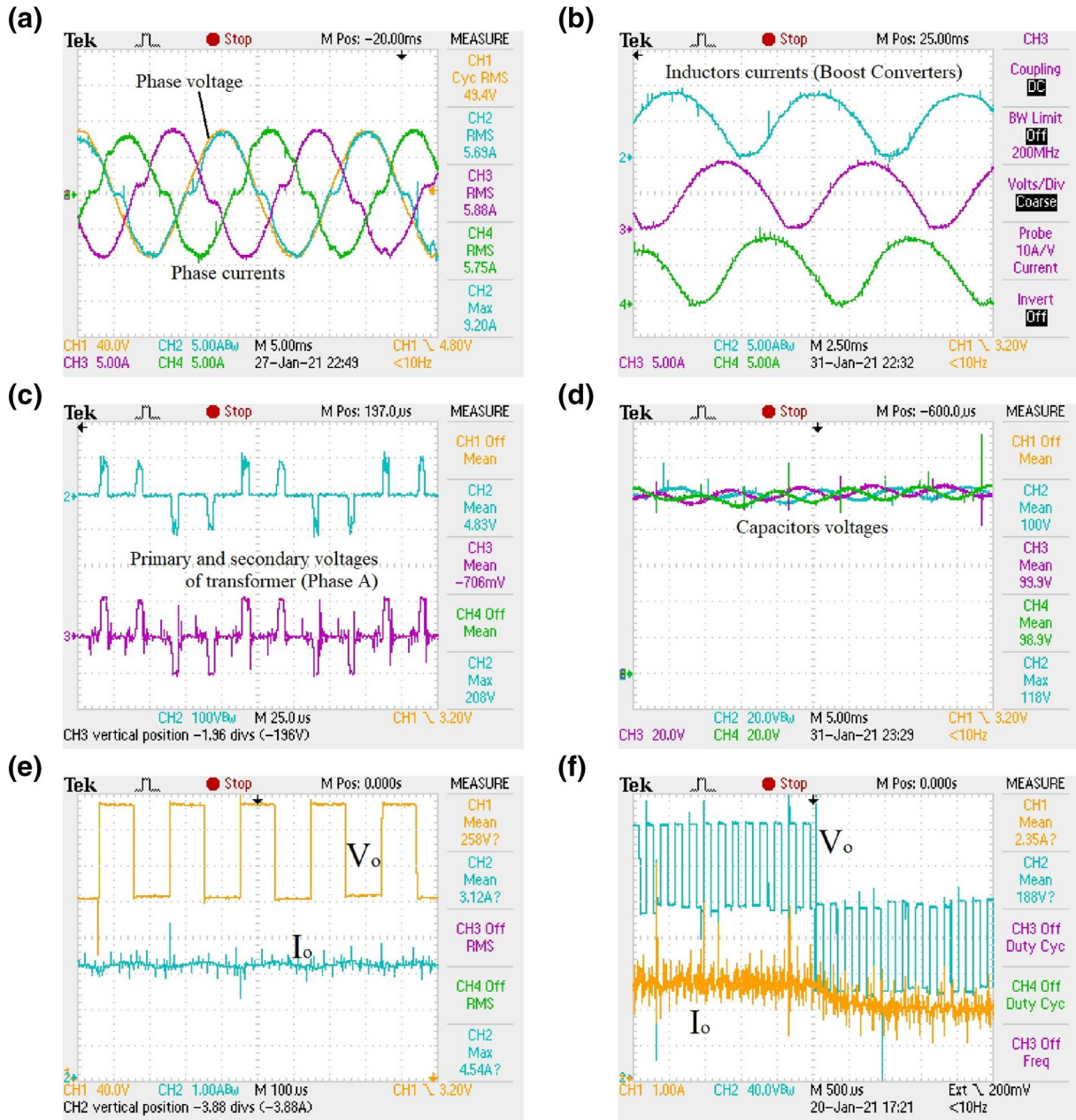
FIGURE 8 The experimental results for the implemented prototype. (a) Grid currents along with one of the phase voltages, (b) the corresponding inductors currents of the three involved isolated boost converters, (c) the primary and secondary voltages of the phase A transformer, (d) the corresponding capacitors' voltages, (e) the output voltage and load current 'I_o' at the charging terminals and (f) dynamic behaviour of the presented converter where the load current reference is decreased from 2.6 to 2 A (step response)

5 | EXPERIMENTAL VALIDATION

A 1 kW scaled-down prototype has been implemented for validation, as shown in Figure 7 with the parameters given in Table 2. In the experimental validation, a resistive load is employed instead of the battery load. With the help of the load current control, a constant current is fed to the resistance to emulate the constant current (CC) charging of the battery, that is, the load current is controlled to track the desired current level as presented in the control system

section. The corresponding experimental results are shown in Figure 8a–e for output current reference of 3.2 A. Figure 8a shows the balanced three-phase AC current drawn from the three-phase AC grid along with one of the phase voltages to show that the grid phase voltage and current are in-phase, where approximately a power factor of 0.9897 is achieved, that is, the PFC feature is verified. The AC current has a %THD of 8.7% in the presented results. The %THD is relatively high due to the employment of three-phase variable AC supply (Variac) as the AC

supply of the proposed charger. The supply AC voltage has 3% total harmonic distortion, increasing the %THD of the drawn current compared to the simulated case study.

The corresponding inductor currents of the involved isolated boost converter modules are shown in Figure 8b, where three-phase rectified currents are achieved synchronized with the phase voltages. The inductor current peak is equal to the peak of the AC grid current, that is, approximately 7 A, as one isolated boost converter module per phase is employed in the experimental validation.

Figure 8c shows the primary and secondary voltages of the involved 1:1 transformer, where the secondary voltage is applied across the diode bridge rectifier to replenish the output capacitor at the same phase. The corresponding capacitors voltages are shown in Figure 8d, where balanced capacitors voltages are achieved with an average value equal to the desired capacitor voltage level, which is 100 V. The corresponding load current (I_o) and the generated voltage across the charging terminals (V_o) are shown in Figure 8e, where an output current with the desired magnitude is successfully generated at the load side, via generating the suitable (V_o). The output DC current has current ripple of 6.6% at 5 kHz.

To check the proposed three-phase EV charger's performance, the load current reference is changed from 2.6 to 2 A (step change), and the output voltage and current responses are monitored. The corresponding variation of output voltage (V_o) and load current (I_o) due to the change of load current reference is shown in Figure 8f, where the closed-loop current control at the load side changes the output voltage reference to achieve the new desired level of the load current. The result shows that

the actual load current tracks the desired load current level successfully.

6 | ASSESSMENT OF THE PROPOSED CHARGER

This section compares the proposed charger and other chargers to show the advantages and disadvantages of the proposed approach compared to the other three-phase topologies presented in the literature. Following assumptions have been taken, where one module per phase for the multimodule topologies is assumed and isolation transformer with turns ratio (1:a) is employed. The terms (V_o, V_{in}, V_p) in the comparison indicate the converter output voltage, the converter input voltage, and the transformer primary voltage, respectively. The comparison is shown in Table 3. The comparison shows that the proposed approach has a lower number of passive elements (inductors and capacitors), which positively affects the charger cost and size. On the other hand, the proposed approach has a higher number of semiconductor devices compared with the other presented topologies but with a lower voltage rating. For example, in Ref. [15], just three switches are needed but with a voltage rating of ($V_o + V_{in}$), which is relatively high compared to the voltage rating of the involved switches in the proposed approach, which approximately equals $V_o/3$. In addition, the proposed approach provides galvanic isolation as well as it can operate in case of input phases' loss, that is, it can operate as one-phase charger or two-phase charger during abnormal operating conditions.

T A B L E 3 Comparison between the proposed charger and other existing three-phase topologies

Point of view	Ref. [18]	[17]	[16]	[15]	The proposed approach
Rectifier bridge	-	12	6	12	12
No. of switches	18	24	6	3	15
No. of conv. diodes	-	12	6	3	15
Voltage stress on switches	12 SWs × V_P, 6 SWs × V_o	12 SWs × V_{in}, 12 SWs × $V_o/2$	$V_o/2 + V_{in}$	$V_o + V_{in}$	Pri side: $V_o/3a$ Sec side: $V_o/3$
Voltage stress on converter diodes	-	$V_o/2$	$V_o/2 + V_{in}$	$V_o + V_{in}$	$V_o/3$
No. of isolating transformers	3	6	-	3	3
No. of inductors	6	6	9	12	3
No. of capacitors	2	12	8	9	3
Galvanic isolation	Yes	Yes	No	Yes	Yes
Soft switching	Yes	No	No	No	No
Operating with a reduced number of phases (phase loss)	No	Yes	No	Yes	Yes
Power flow	Bidirectional	Unidirectional	Unidirectional	Unidirectional	Unidirectional

7 | CONCLUSION

In this work, a novel three-phase unidirectional off-board EVs fast charger is proposed based on an isolated boost converter and unidirectional half-bridge submodules (i.e. cascaded DC–DC buck converters). Parallel-in parallel-out isolated boost converter is employed to share the current among them, which reduces the current rating of the involved modules and reduces the overall ohmic losses of the charger. The cascaded DC–DC buck converters at the charging terminals provide the suitable charging voltage, ensuring injecting the desired current into the EV battery. The proposed approach provides the desired charging current at the load side while drawing three-phase balanced AC currents at the AC grid side. Compared to other three-phase topologies, the proposed approach has a lower number of passive elements (inductors and capacitors), which positively affects the charger cost and size. The proposed topology has a higher number of semiconductor devices but with a lower voltage rating. In addition, in case of one- or two-phase loss, the proposed architecture can continue operating successfully with the other healthy phases. An efficiency of 95% is achieved for the proposed charger under the rated condition (25 kW). The proposed closed-loop controllers ensure operating with (i) balanced voltages of the involved boost converter output capacitances, (ii) PFC at the AC input side, (iii) drawing balanced three-phase current at the AC side, and (iv) injecting desired to charge current to the EV battery. All of these features are achieved via employing the proposed closed-loop controllers for the proposed architecture. Simulation and experimental results validate the viability of the mentioned claims.

DATA AVAILABILITY STATEMENT
The data that support the findings of this study are available from the corresponding author upon reasonable request.

ORCID
Ahmed Elserougi https://orcid.org/0000-0002-8961-3051
Ibrahim Abdelsalam https://orcid.org/0000-0002-4140-1711

REFERENCES
1. Blanning, B.: The economics of EVs and the roles of government. In: Proceedings of the 2013 World Electric Vehicle Symposium and Exhibition (EVS27), Barcelona, Spain, 17–20 November, pp. 1–6. (2013)
2. Ryan, C., et al.: Advanced electric vehicle fast-charging technologies. Energies. 12(1839), 1–26 (2019)
3. Ronanki, D., Kelkar, A., Williamson, S.S.: Extreme fast charging technology—prospects to enhance sustainable electric transportation. Energies. 12(3721), 1–17 (2019)
4. Ben Sassi H., et al.: V2G and Wireless V2G concepts: state of the art and current challenges. International Conference on Wireless Technologies, Embedded and Intelligent Systems (WITS). (2019)
5. Du, Y., et al.: Review of high power isolated bi-directional DC-DC converters for PHEV/EV DC charging infrastructure. In: Proceedings of the IEEE Energy Conversion Congress Exposition, pp. 553–560 (2011)
6. Chen, H., Wang, X., Khaligh, A.: A single stage integrated bidirectional AC/DC and DC/DC converter for plug-in hybrid electric vehicles. In Proceedings of the IEEE Vehicle Power Propulsion Conference, pp. 1–6 (2011)
7. Tan, N., Abe, T., Akagi, H.: Design and performance of a bidirectional isolated DC–DC converter for a battery energy storage system. IEEE Trans. Power Electron. 27(3), 1237–1248 (2012)
8. Lee, C.S., et al.: Study on 1.5 kW battery chargers for neighborhood electric vehicles. In: Proceedings of the IEEE Vehicle Power and Propulsion Conference, pp. 1–4 (2011)
9. Aguilar, C., et al.: An integrated battery charger/discharger with power-factor correction. IEEE Trans. Ind. Elect. 44(5), 597–603 (1997)
10. Musavi, F., et al.: Evaluation and efficiency comparison of front-end AC–DC plug-in hybrid charger topologies. IEEE Trans. Smart Grid. 3(1), 413–421 (2012)
11. Garcia, O., et al.: Automotive dc–dc bidirectional converter made with many interleaved buck stages. IEEE Trans. Power Electron. 21(3), 578–586 (2006)
12. Ni, L., Patterson, D.J., Hudgins, J.L.: High power current sensorless bidirectional 16-Phase interleaved DC–DC converter for hybrid vehicle application. IEEE Trans. Power Electron. 27(3), 1141–1151 (2012)
13. Singh, B., et al.: A review of three-phase improved power quality ac–dc converters. IEEE Trans. Ind. Electron. 51(3), 641–660 (2004)
14. Manjrekar, D.M., Steimer, K.P., Lipo, T.A.: Hybrid multilevel power conversion system: a competitive solution for high-power applications. IEEE Trans. Ind. Appl. 36(3), 834–841 (2000)
15. Hussein, B., Abdi, N., Massoud, A.: Development of a three-phase interleaved converter based on SEPIC DC–DC converter operating in discontinuous conduction mode for ultra-fast electric vehicle charging stations. IET Power Electron. 14, 1889–1903 (2021)
16. Costa, P., et al.: Unidirectional three-phase voltage-doubler SEPIC PFC rectifier. IEEE Trans. Power Electron. 36(6), 6761–6773 (2021)
17. Choi, S.-W., et al.: Interleaved isolated single-phase PFC converter module for three-phase EV charger. IEEE Trans. Veh. Technol. 69(5), 4957–4967 (2020)
18. Singh, A.K., et al.: A soft switching single stage isolated three phase bidirectional PFC converter for electric vehicles charging. 2019 North American Power Symposium (NAPS), Wichita, KS, USA, 13–15 October. (2019)
19. Choe, G.Y., et al.: A bidirectional battery charger for electric vehicles using photovoltaic PCS systems. In: Proceedings of the IEEE Vehicle Power Propulsion Conference, pp. 1–6 (2010)
20. Gallardo-Lozano, J., et al.: Three-phase bidirectional battery charger for smart electric vehicles. In: Proceedings of the International Conference of Workshop Compatibility Power Electron, pp. 371–376 (2011)
21. Yilmaz, M., Krein, P.T.: Review of battery charger topologies, charging power levels, and infrastructure for plug-in electric and hybrid vehicles. IEEE Trans. Power Electron. 28(5), 2151–2169 (2013)
22. Valascho, R., Abdel-Rahman, S.: Digital PFC CCM boost converter, 300 W design example using XMC1400 microcontroller. Infineon Application Note (AN_201602_PL30_015). (2016)

> **How to cite this article:** Elserougi, A., Abdelsalam, I., Massoud, A.: An isolated-boost-converter-based unidirectional three-phase off-board fast charger for electric vehicles. IET Electr. Syst. Transp. 12(1), 79–88 (2022). https://doi.org/10.1049/els2.12039